



Evaluation of GNSS ionosphere prediction models Klobuchar-GPS, NTCM-G, and BDGIM: methodology and results for 2021–2024

Lambert Wanninger¹ · Kim Thiemann¹

Received: 13 February 2025 / Accepted: 2 June 2025
© The Author(s) 2025

Abstract

As part of their satellite navigation messages, GPS, Galileo, and BDS broadcast coefficients of ionosphere prediction models. These models are intended to be used for the improvement of single-frequency code-based positioning. We compared vertical electron content derived from these models with those of the more accurate post-processing ionosphere model produced by the International GNSS Service (IGS). On a global scale and for the time period 2021–2024, the Klobuchar-GPS model corrects on average about 59% of the vertical ionospheric delays, the NTCM-G model and a slightly modified BDGIM model give a correction rate of about 74%, while the combination of the latter two models gives a correction rate of 77%. In the case of strong geomagnetic storms with large effects on the ionospheric total electron content, the performance of the prediction models degrades and the global daily correction rates may even drop to below 50%. Single-frequency GNSS receivers with access to all GNSS are recommended to apply ionospheric corrections based on the ionosphere model coefficients and algorithms of Galileo/NTCM-G or BDS/modified BDGIM, or a combination of both. The Klobuchar-GPS model should serve as a backup in case that Galileo and BDS navigation messages are not available.

Keywords Ionosphere prediction models · Vertical total electron content (VTEC) · Global electron content (GEC) · Geomagnetic storms

Introduction

In single-frequency GNSS positioning, ionosphere induced signal delays are one of the main error sources. In order to mitigate ionospheric effects on stand-alone positioning results, most GNSS broadcast coefficients of ionosphere prediction models with their satellite navigation messages. The oldest such model is the one of GPS which was designed to provide a correction for approximately 50% RMS of the ionospheric range error (Klobuchar 1987). Nowadays, more such prediction models are available. The most promising models are Nequick G / NTCM-G of Galileo and BDGIM of BDS.

These ionosphere prediction models are intended for single-frequency stand-alone code-based GNSS positioning. Dual-frequency ionospheric corrections will always provide a much higher correction rate but require costlier receivers.

Regional differential code-corrections will also be superior to any prediction models but depend on additional infrastructure. More accurate real-time ionosphere corrections, as e.g. from satellite-based augmentation systems (SBAS), are not available globally. Hence, for many GNSS-receivers the application of corrections from these prediction models are the first choice for ionospheric corrections.

Ionosphere prediction models will never be accurate enough to be useful for carrier phase positioning in the form of single-frequency precise point positioning (PPP) or dual-frequency PPP with ambiguity fixing. These applications require real-time models of satellite-individual slant total electron content (STEC).

There are several approaches to evaluating ionosphere models. The most often applied techniques include:

- Compare with a more accurate GNSS ionosphere model of vertical total electron content (VTEC): many studies use the final model of the International GNSS Service (IGS) as the reference (e.g. Li et al. 2018; Zhu et al. 2019; Yasyukevich et al. 2023).

✉ Lambert Wanninger
lambert.wanninger@tu-dresden.de

¹ Geodetic Institute, TU Dresden, 01062 Dresden, Germany

- Compare with VTEC estimates derived from dual-frequency observations of other satellite systems, e.g. of satellite altimeters or DORIS: These systems integrate the ionospheric electron content up to the satellite orbital height of e.g. 1340 km (altimeter and DORIS onboard of TOPEX, Jason-1/-2/-3) and so, part of the plasmaspheric ionization is not captured (Azpilicueta and Brunini 2009). Both systems provide no dense global coverage of ionospheric observations: altimeters are restricted to ocean areas and DORIS to the surroundings of the just about 50 transmitting stations on the Earth's surface. Furthermore, altimeter derived VTEC may suffer from biases due to uncalibrated instrumental delays (Dettmering et al. 2011; Azpilicueta and Nava 2021).
- Compare models with dSTEC estimates based on dual-frequency carrier phase observations of full satellite passes: These observed variations of STEC along satellite passes (dSTEC) are free of biases and the most accurate ionospheric observations which can be obtained from GNSS or DORIS signals (Hernández-Pajares et al. 2017; Liu et al. 2023). They are well suited for model evaluations in areas with sufficient ground stations.
- Apply the corrections to single-frequency GNSS observations and evaluate the remaining errors in the positioning domain: This requires an appropriate handling of all other error sources. The results may differ depending on the selected positioning mode: code-based standard positioning (Cahuasquí et al. 2022; Setti et al. 2025) or carrier phase-based single-frequency precise point positioning.

Our intention was to perform an evaluation of the GNSS ionosphere prediction models globally without regional gaps and continuously over an extended period of time. We decided to compare VTEC values derived from prediction models with VTEC values from the more accurate post-processed IGS model.

All broadcast models considered in this study are single-layer models. They assume that all free electrons are contained in a shell of infinitesimal thickness at a fixed altitude H_f of 350 ... 450 km. The parametrization of the models and consequently the kinds of model coefficients transmitted as part of the satellite navigation message differ considerably.

The task of the single-layer models is to provide delay corrections at the ionospheric pierce points (IPP) which are the intersection points of the signal paths from the broadcasting satellites to receivers on or near the Earth's surface. The correction algorithms consist of two steps: (1) computation of VTEC or vertical signal delay at the IPP and (2) computation of a slant factor to convert vertical to slant TEC or signal delay. In this study, we evaluated the quality of VTEC predictions. We did not consider any deviations introduced by the slant factors.

There are many studies that have used a similar approach, but they are often limited to particular regions or a shorter time period. Our evaluation covers the global ionosphere and considers the time period 2021–2024, from solar minimum to solar maximum conditions of solar cycle 25. As an improvement over other studies, we have refined the evaluation method and the statistical indices with respect to the proper latitudinal weighting of VTEC deviations. We propose combining the corrections from the two best models to achieve even more accurate results. We have tested this idea and present the results.

In the following section, the GNSS ionosphere broadcast models are introduced. Subsequently, we discuss the use of the IGS model as a reference model and the IONEX format as a storage model for VTEC. We will briefly introduce the development of the ionosphere from 2021 to 2024. The main part of the paper deals with our evaluation method, the presentation of the results and their discussion.

GNSS ionosphere prediction models

GPS

The first and oldest GNSS ionosphere broadcast model is the one of GPS. The GPS ionospheric correction algorithm (ICA), which is commonly referred to as Klobuchar model and which in this paper we will call GPS model, is driven by 8 broadcast coefficients which occupy 64 bits of the satellite navigation message (Table 1). They are the coefficients of two polynomial functions of the receiver geomagnetic latitude. These third-degree polynomials describe amplitude and period of a semi-cosine function (Klobuchar 1987). Further fixed parameters include the cosine peak at 14 h

Table 1 The GNSS ionosphere prediction models evaluated in this study

Model	Number of coefficients and bits	Model outcome considered in this study	Update rate	Computational load with respect to GPS model	References
GPS	8; 64	delay on GPS L1 (1575.42 MHz) in units of s	up to once per day	1	IS-GPS 2022
NTCM-G	3; 36	VTEC in units of TECU	up to once every 12 h	5	GSC 2022
BDGIM	9; 74	VTEC in units of TECU	up to once per hour	60	CSNO 2019

local time and a nighttime delay at GPS L1 frequency of 5 ns. The latter corresponds to a minimum VTEC of 9.2 TECU since the conversion of the frequency-dependent ionospheric signal delay D_f^{iono} in s to *TEC* in TECU, or vice versa, is (Morton et al. 2020):

$$D_f^{iono} = \frac{40.3}{c_0 f^2} TEC \quad (1)$$

with the vacuum velocity c_0 in m/s and the signal frequency f in Hz.

The GPS navigation messages are usually updated once every two hours. This, however, is not true for the 8 ionospheric coefficients. They stay unchanged for longer periods of time. Klobuchar (1987) states that they are updated once every 10 days, or sometimes more frequently, if large solar flux changes occur. Morton et al. (2020) report that they are updated once every 6 days. We found that until mid-2021 the updates took place every 10 days. Afterwards they occurred more often: up to once per day.

The Klobuchar model is designed to reduce calculation complexity, especially through simplifying assumptions of the geometric functions (Klobuchar 1987). We determined the computational load of the evaluated prediction models by coding them in FORTRAN with special attention to run-time efficiency. We tested the models on two different computer systems with different processing power. Although the absolute run-time values differed greatly, the run-time ratios with respect to the GPS model were highly consistent. Table 1 reports these ratio values to provide information on the computational load of each model.

Galileo

The satellites of the European Galileo system transmit three coefficients of a second-degree polynomial of the modified dip latitude at the location of the receiver. They are used to compute a single model input value: the effective ionization level A_z (EUSpace 2023). This part of the satellite navigation message is updated at least once per day (Morton et al. 2020) which is confirmed by our results for 2021–2024, with the lowest update rate being once per day and the highest update rate being once every 12 h.

The original ionosphere model to be used with A_z is called NeQuick G (EC 2016). NeQuick G ionospheric delay corrections are obtained by integrating electron densities along the signal path from the satellite to the receiver. It is based on a three-dimensional electron density model and not on a single-layer model. One of the major drawbacks of NeQuick G is its computational load which we estimated to be around 200 times higher than that of the GPS model.

In order to provide a model with less computational complexity, GSC (2022) published an alternative model

called NTCM-G. It is based on the Neustrelitz Total Electron Content (NTCM) model, adapted to the proxy measure of the solar activity level $Azpar$ which is determined from the three coefficients broadcast in the Galileo navigation message. It belongs to the group of single-layer models and comes with a mapping function for the conversion of VTEC to STEC. VTEC is determined by multiplying 5 functions which describe (1) the diurnal, semi-diurnal and tar-diurnal variations, (2) annual and semi-annual variations, (3) dependence on geomagnetic latitude, (4) equatorial crest region, and (5) solar cycle variations (Hoque et al. 2019). The functions are driven by using 12 fixed parameters which were determined by fitting the model to post-processed global VTEC estimates of the Center for Orbit Determination in Europe (CODE), which serves as one of the analysis centers of the IGS. The CODE data used covers the years 2013–2017 and includes high and low solar activity conditions of the decreasing phase of solar cycle 24 (Hoque et al. 2019).

Comparisons of the performances of the two different models driven by Galileo's coefficients conclude in several different tests that NTCM-G performs better or as good as NeQuick G (Hoque et al. 2019), NTCM-G performs similarly to NeQuick G (GSC 2022), NTCM-G's positioning performance is better than the one of NeQuick G in a one-month period of perturbed solar and geomagnetic activity, but also in a month of quiet conditions (Cahuasquí et al. 2022), and based on a sample size of just 4 days: NTCM-G performs slightly better in low- and medium-solar-activity conditions, while NeQuick G has better performance with intense solar activity (Gioia et al. 2023).

From these research results, we conclude that that NTCM-G performs similarly to NeQuick G with respect to VTEC accuracy and positioning performance. But the computational load of these two models is very much different. The computational effort required for NeQuick G is approximately 65 times (Hoque et al. 2019; Cahuasquí et al. 2022) or 50 times (Gioia et al. 2023) higher than for NTCM-G. From our own model realizations, we concluded that the computational effort required for NeQuick-G is approximately 40 times higher than for NTCM-G. With a similar performance in accuracy but a much higher computational efficiency, we have decided that the NTCM-G model should represent the Galileo ionosphere correction in this study.

BDS

The regional Chinese BDS-2 broadcasts Klobuchar-like ionosphere model coefficients. In the global BDS-3, nine coefficients of a second ionosphere model, called BDGIM, were added to the navigation message (CSNO 2019). BDGIM belongs to the group of single-layer models and

comes with a mapping function for the conversion of VTEC to STEC. The 9 values represent the coefficients of a spherical-harmonic function model based on normalized Legendre functions up to degree and order 2. Besides this variable part of the model, there are non-broadcast fixed coefficients for higher degrees and orders and 12 selected periods from sub-diurnal up to 11 years.

We determined the maximum update rate of the BDGIM broadcast model coefficients to be once per hour. The computational load of BDGIM is about 60 times higher than that of the GPS model and about 12 times higher than that of NTCM-G.

Early evaluations of BDGIM by Zhao et al. (2020), Guo et al. (2020), and Zhang et al. (2022) show that the accuracy performance of BDGIM is far superior to that of the Klobuchar-like BDS model. We have therefore chosen BDGIM for the evaluation in this study.

Other systems and models

No ionosphere model coefficients are broadcast as part of the GLONASS FDMA navigation message. But the more recently defined CDMA navigation message contains 3 coefficients (31 bits) which are used to adapt a three-dimensional electron density model to the predicted ionospheric conditions. Ionospheric corrections are computed by integrating electron densities along the signal path from the satellite to the receiver (JSC 2016). Due to the lack of model coefficients, we were not able to include this model in our evaluation.

Further broadcast prediction models exist or will exist but they are all limited to certain regions and were not included in our evaluation. QZSS transmits coefficients of Klobuchar-like models, one set for Japan and another set for the wider area of the longitude range 90 to 180 deg (QZSS 2021). The Indian NavIC system transmits regional ionospheric prediction models in three different kinds of parametrization: gird model, Klobuchar-like and NeQuick-like (ISRO 2017).

Part of the satellite messages of the satellite-based augmentation systems (SBAS) contain real-time ionospheric corrections in gridded form. They are only available for limited regions and were therefore not included in this study. Furthermore, being real-time products and not predicted models, they belong to another class of ionosphere models not considered in this study.

The IGS ionosphere model as the reference model

The IGS has produced global ionosphere VTEC maps since 1998. Up to 8 Ionosphere Associate Analysis Centers (IAACs) compute ionosphere VTEC maps in post-processing mode based on multi-frequency GNSS

observations of stations of the IGS network and other permanent reference stations.

The final IGS VTEC maps are computed as weighted averages of the individual solutions. The weights are determined from the inverse root mean square of errors of observed STEC variations (dSTEC) which are obtained from GNSS dual-frequency carrier phase observation of a certain subset of stations (Hernández-Pajares et al. 2009; Orús et al. 2005). An example of such weights is given by Hernández-Pajares et al. (2009).

The analysis of the daily files of the final IGS ionosphere VTEC maps for 2021–2024 revealed that in 2021 and until almost the end of 2022 the solutions of 4 IAACs were fed into the combination process. After that, the number of IAAC solutions used dropped to only 3 (Fig. 1). The involved IAACs are: Center of Orbit Determination in Europe (CODE), Jet Propulsion Laboratory (JPL), Polytechnic University of Catalonia (UPC), and until end of 2022 European Space Agency (ESA).

The IGS VTEC maps are based on the observation data of hundreds of permanent GNSS stations. Over the period 2021–2024, the maximum number of stations reached slightly above 400 in early 2021, it dropped to about 300 at the end of 2022 when the number of IAAC solutions was reduced from 4 to 3 (Fig. 1). The increase of observation stations in early 2024 was caused by an increase of stations processed by JPL.

Note that the observation stations are not well distributed on the Earth's surface. At some locations, the observations of more than one receiver are processed, although they provide redundant data with respect to the ionosphere. In other areas there is a lack of ground stations. In order to visualize the spatial distribution of the ionosphere sampling, we analyzed the ionospheric pierce points of all observation data of day 146 in 2021 (420 observation stations) and of day 203 of 2024 (340 observation stations). Figure 2 depicts the number of observation stations per ionospheric pierce point with

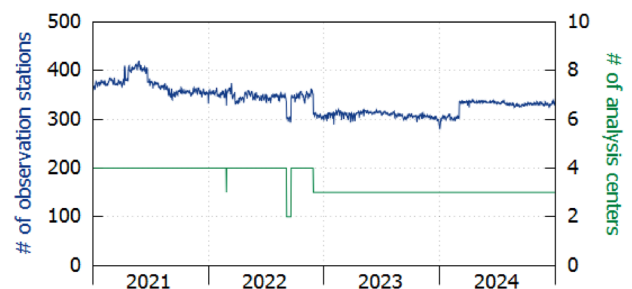


Fig. 1 The daily IGS ionosphere VTEC product is a combination of the results of a number of analysis centers (green line) and based on the observations of hundreds of GNSS reference stations (blue line)

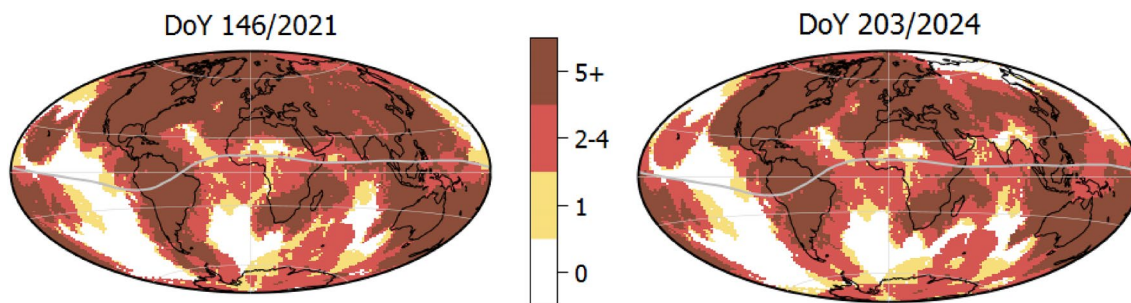


Fig. 2 Number of observation stations per Ionospheric Pierce Point of the IGS single layer ionosphere model (single layer height: 450 km, grid size of 350 km × 350 km at single layer height, GPS + Galileo constellation, elevation mask angle of 5 deg)

a spatial resolution of 350 × 350 km². The color coding highlights areas:

- without any observations, where the models depend on spatiotemporal interpolation only,
- with observations of a single station, i.e. without redundancy,
- with 2 to 4 stations, which we consider as the optimum, and
- with 5 and more stations, i.e. with abundant redundancy.

Areas without any observations are mainly found over the oceans, off the coasts and islands with permanent GNSS stations. The largest coverage gaps are found over parts of the Pacific Ocean, over the southern Atlantic Ocean, and to a smaller extent over the southern Indian Ocean. From 2021 to 2024 the areas without any observations significantly increased due to the loss of IGS stations in Siberia.

Every VTEC value of the IGS ionosphere models is accompanied by its RMS, estimated from the residuals of the original IAAC models with respect to the combined model. In order to evaluate the spatial distribution of these RMS values, we averaged the squared RMS values of every grid point over periods of complete years (Fig. 3). First of all, RMS values increase with increasing ionization. This can be seen in the annual results from 2021 to 2024 which reflect the increase of solar activity. It is also obvious in the latitudinal distribution of the RMS values with its highest values in the equatorial region. Second, the RMS values depend on the coverage with observations. The highest RMS values are found in the Pacific equatorial region where observations are lacking. The lowest RMS values are found in those parts of the mid-latitude regions where many GNSS permanent stations are available.

The evaluation of the combined IGS VTEC products is done by comparison with VTEC values provided by dual-frequency altimeters on board JASON satellites. Hernández-Pajares et al. (2009) determined average standard deviation and average RMS errors of about 4.5 TECU each over the

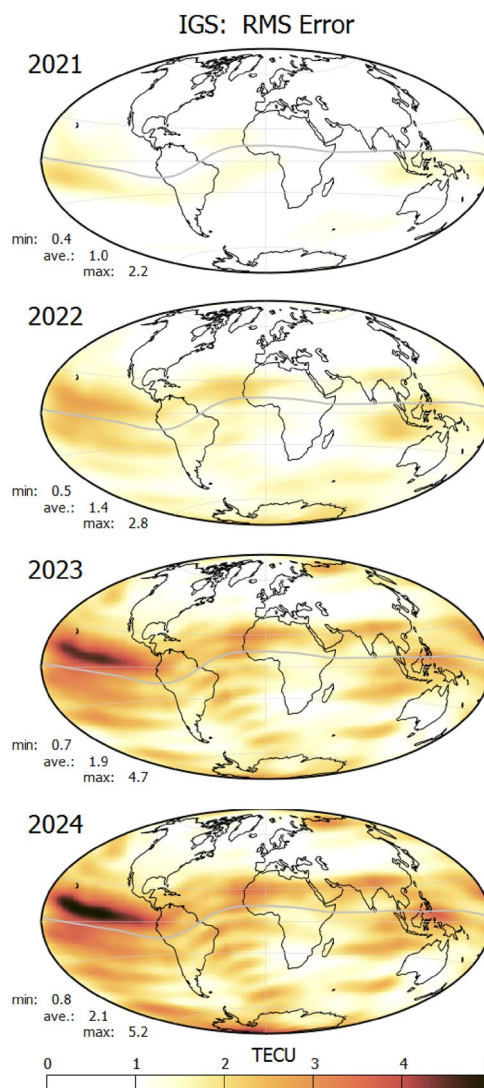


Fig. 3 Spatial distribution of the annual mean IGS VTEC RMS values

oceans for the time period from end of 2002 to 2007. This corresponds to a relative RMS/VTEC of 20%. Applying the same method for one month of data in the solar cycle minimum (January 2021) resulted in a standard deviation of about 2.4 TECU (Krankowski and Hernández-Pajares 2021). The IGS states that their final VTEC product has an accuracy of 2 – 8 TECU (Johnston et al. 2017).

In conclusion, an accuracy of the final IGS ionosphere model of a few to some TECU can be expected. The accuracies are subject to large spatial and temporal variations depending on the ionization level and also on the availability of permanent GNSS reference station observations in the region. As a post-processing product, it will be superior to all the prediction models evaluated in this paper and it can serve as the reference VTEC model.

VTEC representation in IONEX format

The IONEX format was defined by Schaer et al. (1998) and has not been changed since. Its main purpose is to store and exchange VTEC maps and corresponding quality measures (RMS values). The format is widely used because it has been used by the IGS analysis centers for their ionosphere products as well as for the rapid and final IGS ionosphere products.

VTEC maps (and their RMS values) are stored in a geographic grid with time intervals of 1 or 2 h or denser. Typical IONEX files contain several maps which cover a whole day.

The IONEX grid is defined with fixed angular distances in latitude (e.g. $\Delta\varphi = 2.5^\circ$) and longitude (e.g. $\Delta\lambda = 5^\circ$) between adjacent grid points (Fig. 4). The longitudinal spacing of adjacent grid points at the height of the single-layer ionosphere model in km is therefore much larger at the equator than in the polar regions. The area A in km^2 represented by a single grid point (Fig. 5) is a function of its latitude φ and $\Delta\lambda$, $\Delta\varphi$ in rad:

$$A(\varphi, \Delta\lambda, \Delta\varphi) = \begin{cases} (R_E + H_I)^2 * \Delta\lambda * \left[\sin\left(\varphi + \frac{\Delta\varphi}{2}\right) - \sin\left(\varphi - \frac{\Delta\varphi}{2}\right) \right], & |\varphi| < 90^\circ \\ (R_E + H_I)^2 * \Delta\lambda * \left[1 - \sin\left(|\varphi| - \frac{\Delta\varphi}{2}\right) \right], & |\varphi| = 90^\circ \end{cases} \quad (2)$$

where R_E is the Earth radius in km (e.g. 6371 km) and H_I is the height of the single-layer ionosphere model in km (e.g. 450 km). For the given example values, at the geographic equator a grid point represents an area of roughly $174 \cdot 10^3 \text{ km}^2$ and at a latitude of $\pm 87.5^\circ$ of just $7 \cdot 10^3 \text{ km}^2$ (Fig. 5). This distortion has to be taken into account in the statistical analysis of the global ionosphere models.

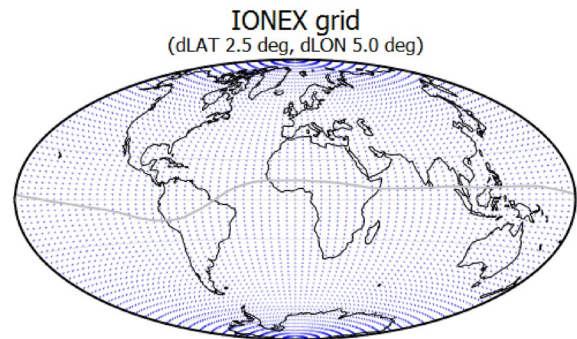


Fig. 4 Spatial distribution of IONEX grid points

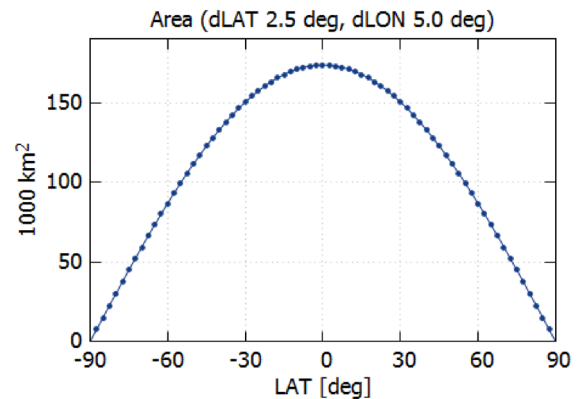


Fig. 5 Latitudinal dependence of the area represented by single grid points

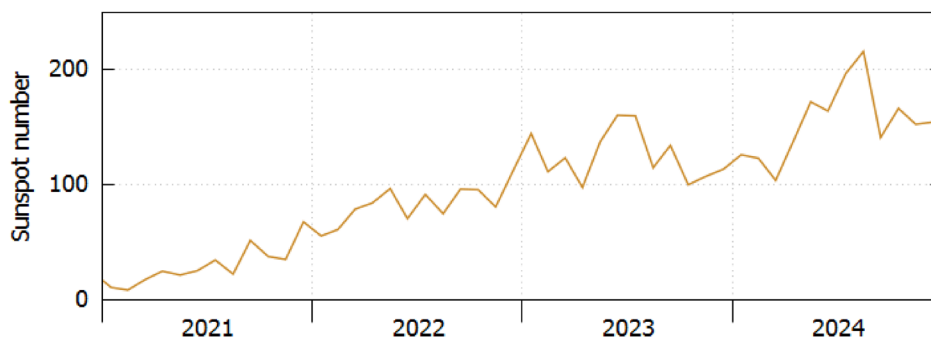
The ionosphere in the years 2021–2024

The properties of the ionosphere in the years 2021–2024 are affected by the increase of solar activity. We are presently in the ascending period of solar cycle 25 which began around

the turn of the year 2019/2020 and is expected to continue until 2030. The time series of monthly mean total sunspot numbers (Fig. 6) shows low but already increasing values in 2021, whereas in 2024 we seem to be close to the maximum of this solar cycle. The time period examined in this paper represents years from low to high solar activity.

Solar activity has a direct effect on the ionization of the Earth’s ionosphere. The ionization level can be derived from global VTEC maps using the concept of the global electron

Fig. 6 Monthly mean total sunspot numbers 2021–2024 (data source: <https://sidc.be/SILSO/>)



content (GEC) (Afraimovich et al. 2008). Based on global VTEC maps, e.g. those of the IGS, GEC is computed by

$$GEC = \sum_{\lambda} \sum_{\varphi} VTEC(\varphi, \lambda) * A(\varphi, \Delta\lambda, \Delta\varphi) \tag{3}$$

where the representative areas A of the grid points are determined according to Eq. 2. GEC is obtained in global electron content units (GECU) which are defined as 10^{32} electrons/ m^2 (Afraimovich et al. 2008). When computing GEC from IGS IONEX files, one has to take into account that these files contain VTEC values at longitude $\lambda = +/- 180^\circ$ twice and that VTEC maps of midnight epochs overlap in subsequent files. Since the IGS IONEX files do not contain values for $\varphi = +/- 90^\circ$, we reused the values for $\varphi = +/- 87.5^\circ$.

An alternative approach to determine GEC can be applied if the global VTEC distribution is modeled by spherical-harmonic functions. Then, the spherical-harmonic coefficient for degree and order 0 represents the global mean VTEC (Schaer 1999) and GEC is computed by:

$$GEC = (R_E + H_i)^2 * 4\pi * 10^{-16} * VTEC_{global}^{mean} \tag{4}$$

This equation is useful, e.g., to determine GEC from BDGIM broadcast model coefficients, where the first coefficient α_1 represents the global mean VTEC.

The daily GEC values from IGS VTEC maps (Fig. 7) show the ionization increase from 2021 to 2024. It is superimposed by a semi-annual period with maxima around the

Fig. 7 Global electron Content (GEC) estimated from 2 hourly IGS VTEC maps and reduced to daily median values



equinoxes and a period of around 27 days in agreement with the solar synodic rotation period.

Another important physical process which affects the ionosphere is caused by geomagnetic storms. Their intensities are generally described by Dst and Kp indices. Dst is an index of magnetic activity derived from a network of near-equatorial geomagnetic observatories. It monitors the equatorial ring current variations (Mayaud 1980). Storms are often classified according to their smallest Dst value (Fig. 8). The planetary geomagnetic Kp index describes the intensity of disturbances in the Earth’s magnetic field. It is derived from observations of multiple subauroral geomagnetic observatories (Matzka et al. 2021). Its purpose is to quantify solar particle radiation by its effects on the Earth’s magnetic field. In order to detect longer lasting events which could have a significant effect on the ionization of the Earth’s upper atmosphere we filtered the 3 h Kp time series with a moving time window of 24 h (Fig. 8). In the time period 2021–2024 the six events with Dst^{min} below -150 nT and large 24 h averaged Kp values occurred in 2023 and 2024, i.e. in years of higher solar activity.

In a later section of this paper, we will look at the effects of these geomagnetic storms on GEC and at the performance of the GNSS prediction models during these events.

Evaluation method

Our evaluation of the GNSS ionosphere broadcast prediction models consists of two major steps (Fig. 9). First, the

Fig. 8 Dst and Kp index values (data sources: <https://wdc.kugi.kyoto-u.ac.jp> and <https://kp.gfz-potsdam.de>, respectively). The original 3 h Kp values have been smoothed with a moving average filter with a window of 24 h. Labels a to f indicate the six strongest geomagnetic storm events in the time period 2021–2024

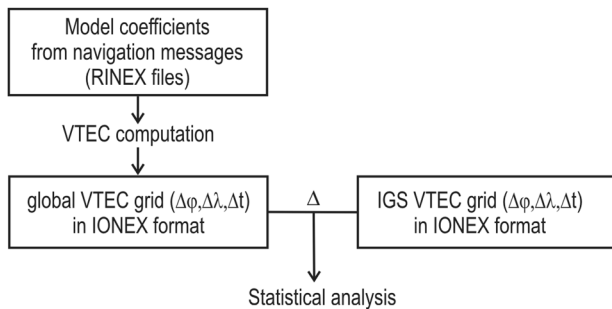
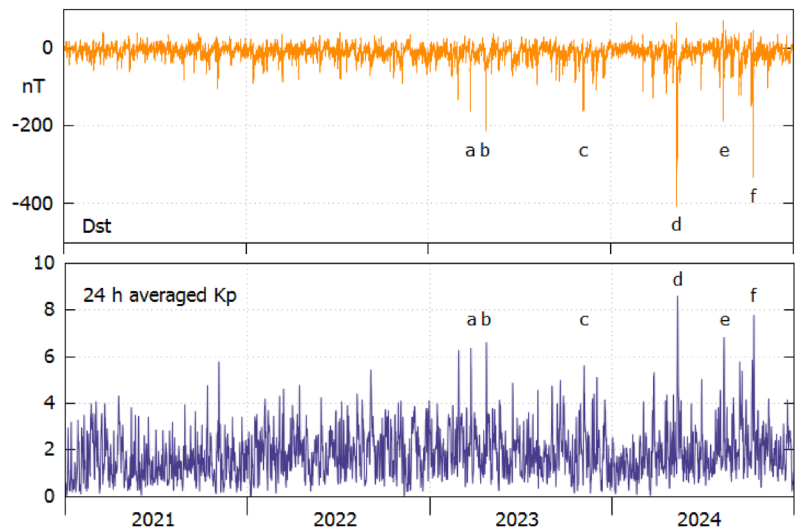


Fig. 9 Workflow of the evaluation of the GNSS ionosphere prediction models

model coefficients from the satellite navigation messages were transformed to VTEC values of a global grid similar to the one used by IGS ($\Delta t = 2$ h, $\varphi_{\max} = \pm 87.5^\circ$, $\Delta\varphi = 2.5^\circ$, $\Delta\lambda = 5^\circ$) and stored in IONEX format. The model coefficients were extracted from RINEX navigation message files. Especially useful were those in format RINEX 4, which have been available since 2022. They are compiled by the German Aerospace Center (DLR) and made available by NASA’s Archive of Space Geodesy Data (CDDIS). For 2021, when RINEX 4 had not yet been defined, satellite navigation message files exist in RINEX 3.04. However, they do not contain model coefficients of BDGIM. Those could be obtained from the Test and Assessment Research Center of the China Satellite Navigation Office (CSNO-TARC) in a modified RINEX 3 format. On very few days, some model coefficients were not included in the RINEX files and we added this information from other RINEX navigation files available at the CDDIS archive.

The transformation step from model coefficients to global VTEC grid values does not apply the model specific

mapping function and makes no use of the model specific single-layer ionosphere height.

In a second step, differences are calculated from the VTEC values of the models being evaluated and the corresponding values of the IGS model and these differences are statistically analyzed. Each grid map contains 5,112 VTEC values. With 12 grid maps per day and 1,461 days in 2021–2024, the number of VTEC values evaluated adds up to around 7.5 million per model.

We calculated bias, RMS error, and correction rate as statistical values. They have often been used in ionosphere model comparisons (e.g. Yuan et al. 2019; Zhu et al. 2019; Setti, et al. 2025), but we modified their computation. When applying them for global VTEC maps it is important to introduce a latitude dependent weighting scheme. Otherwise, with equal weighting of the differences at all grid points, the polar regions will be overweighted and the effect of the equatorial region will be underweighted. Therefore, we weight the grid point VTEC differences according to their representative areas as derived in Eq. 2 and depicted in Fig. 5.

The following equations contain summations in space and time. Some results shown in the result section of this paper just used the summation in time.

Model bias in TECU:

$$B^{Model} = \frac{1}{\sum_A} \sum_{\lambda} \sum_{\varphi} \sum_t [VTEC^{Model}(t, \varphi, \lambda) - VTEC^{IGS}(t, \varphi, \lambda)] * A(\varphi, \Delta\lambda, \Delta\varphi) \tag{5}$$

Negative bias values indicate an underestimation of the electron content, positive values an overestimation. The global average bias with respect to the IGS reference model stands for the difference in global mean VTEC, which is

directly related to the GEC difference between evaluated model and reference model as described by Eq. 4.

Model RMS error in TECU:

$$R^{Model} = \sqrt{\frac{1}{\sum A} \sum_{\lambda} \sum_{\varphi} \sum_t [VTEC^{Model}(t, \varphi, \lambda) - VTEC^{IGS}(t, \varphi, \lambda)]^2} \tag{6}$$

* $A(\varphi, \Delta\lambda, \Delta\varphi)$

In contrast to a standard deviation, the RMS error contains the influence of the bias.

Correction rate of the model:

$$C^{Model} = \frac{1}{\sum A} \sum_{\lambda} \sum_{\varphi} \sum_t \left[1 - \frac{|VTEC^{Model}(t, \varphi, \lambda) - VTEC^{IGS}(t, \varphi, \lambda)|}{VTEC^{IGS}(t, \varphi, \lambda)} \right] \tag{7}$$

* $A(\varphi, \Delta\lambda, \Delta\varphi)$

Correction rate values were not determined when reference VTEC values of the IGS model were smaller than a threshold of 2 TECU, as the correction rate values become unstable for small reference VTEC values. Such small VTEC grid values mainly occur at solar minimum. In 2021, 4.1% of all grid points showed VTEC values below this threshold. In 2022, it was 0.8%. In 2023 and 2024, it was less than 0.1%.

In rare cases, negative correction rate values are estimated. They indicate a severe VTEC overestimation by the evaluated model. Applying these VTEC values as corrections produces worse results than applying no ionosphere corrections at all.

Note that these correction rates refer to vertical TEC and are not influenced by the inaccuracies of the mapping functions of the evaluated model and of the reference model. The correction rates of slant TEC are expected to be smaller.

Results and their interpretation

GPS

The statistical results for the GPS model (Fig. 10) show significant differences with latitude. In the polar regions, VTEC is far overestimated especially in years of low ionization (2021, 2022). This is caused by the fixed minimum VTEC value of 9.2 TECU. It does not seriously affect the RMS error, which remains small, but it affects the correction rate with values below 30% and even negative values.

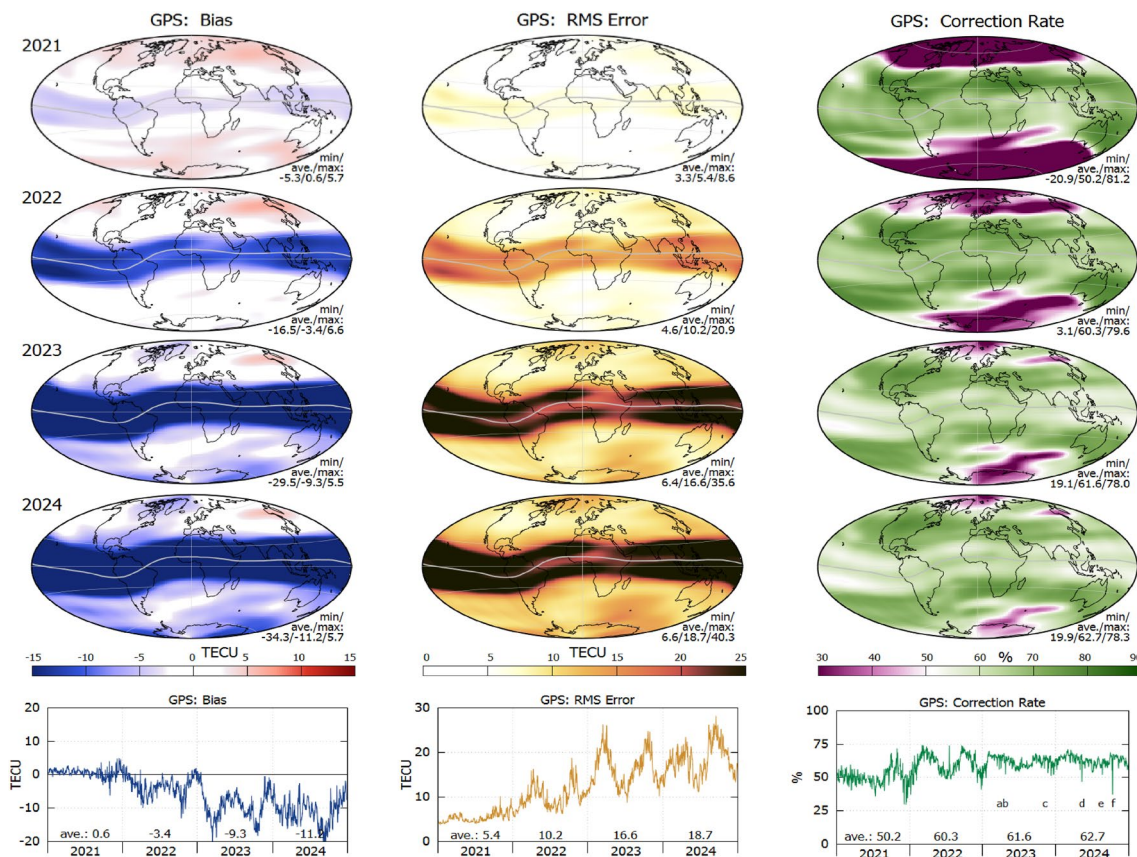


Fig. 10 Spatial distribution (annual averages, upper panels) and temporal distribution (daily global averages, bottom panels) of the statistical values bias (left), RMS error (center), and correction rate (right) for the GPS model

In the equatorial region, VTEC is underestimated: in 2021 by a few to some TECU, increasing to over 20 TECU in 2024 (upper left panels of Fig. 10). These large biases have a direct effect on the RMS errors, which exceed 20 TECU in the regions of the equatorial ionization anomalies (upper central panels of Fig. 10) and especially around the time of the equinoxes (bottom central panel of Fig. 10), the seasons with highest ionization level (cp. Figure 7). The large biases also effect the correction rate which is significantly smaller in the equatorial region as compared to the mid-latitudes (upper right panels of Fig. 10).

The daily globally averaged RMS errors (bottom center panel of Fig. 10) show a strong seasonal variation. RMS errors are highest around the equinoxes, especially from 2022 to 2024. Correction rates are highest around the equinoxes, especially in 2022. The global average correction rate is around 50% in 2021, the year with lowest ionization level. With higher VTEC values the correction

rate increases and reaches values around 60% on global average.

Smallest biases, smallest RMS errors and highest correction rates are found in the mid-latitudes and within the mid-latitudes in the area of the continental USA. There, the correction rates of the GPS model reach 61.5% (2021), 71.9% (2022), 74.2% (2023), and 73.3% (2024) and are much higher than in other world regions, including other mid-latitude regions.

The figure of the daily globally averaged correction rates (bottom right panel of Fig. 10) contains labels a to f to indicate the occurrence of geomagnetic storms. Whereas, their effects are hardly visible in the time series of the globally averaged biases and the globally averaged RMS errors, some of them have caused a tremendous decrease of the correction rates. The effects of these storms are discussed in more detail in a later section of this paper.

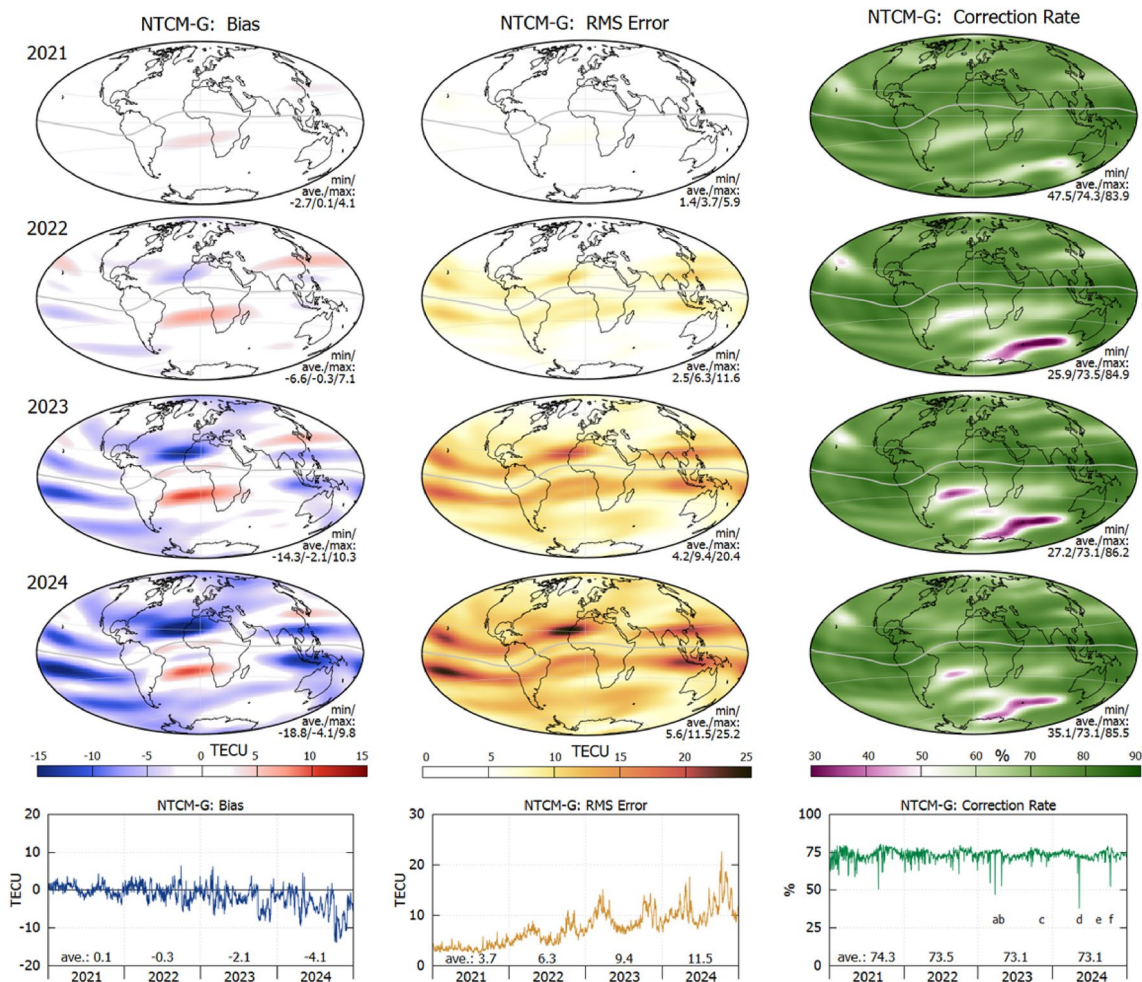


Fig. 11 Spatial distribution (annual averages, upper panels) and temporal distribution (daily global averages, bottom panels) of the statistical values bias (left), RMS error (center), and correction rate (right) for model NTCM-G

NTCM-G

Biases of the NTCM-G model with respect to the IGS reference model remain on a low level but increase with increasing ionization (left panels of Fig. 11). On a global average, a slight underestimation of VTEC is present, reaching 4.1 TECU in 2024. Larger biases (up to around +/- 10 TECU) exhibit a latitudinal and longitudinal distribution and are mainly seen in the regions of the equatorial ionization anomalies.

The RMS errors increase from 2021 to 2024 (central panels of Fig. 11). RMS errors are larger in the equatorial region as compared to mid-latitude and polar regions. Seasonal variations with highest values around the equinoxes are visible (bottom central panel of Fig. 11).

There are regional differences in the correction rates, with areas of lower values (below 50%) located primarily in the southern hemisphere over the southern Atlantic and Indian Oceans.

The daily global averaged correction rates (bottom right panel of Fig. 11) are continuously on a level of around 73%. They show no variation with increasing solar activity and very little seasonal variation. On single days, however, severe drops of the correction rates to less than 60% can be observed. Some of them can be attributed to the effects of geomagnetic storms, the largest storms being labeled with letters a to f. The effects of these storms are discussed in more detail in a later section of this paper.

BDGIM

Calculation of BDGIM STEC or VTEC can result in negative electron content values. Computing BDGIM VTEC values for the IONEX grid, negative values were obtained for 0.4% (2021), 1.0% (2022), 0.8% (2023), and 3.5% (2024) of all grid points which may indicate an increase in the number of negative values with increasing solar activity. Most of

the negative VTEC values were observed at higher latitudes of the southern hemisphere from April to September. To a smaller extent, they also occur in higher latitudes of the northern hemisphere from November to February (Fig. 12). These findings for BDGIM are in very good agreement with the results of Zhang and Zhao (2023), who analyzed the occurrence of negative VTEC values when using spherical harmonic expansion models.

In order to substitute these unrealistic values by more reasonable ones, we revised the method suggested by Wang et al. (2021) and substituted very small and negative BDGIM VTEC values by a fifth of the predicted mean global VTEC:

$$VTEC^{mBDGIM} = \max(VTEC^{BDGIM}, 0.2 \cdot \alpha_1) \tag{8}$$

where α_1 denotes the first BDGIM model coefficient, which is the spherical-harmonic coefficient for degree and order 0, i.e. the predicted mean global VTEC. With this procedure, we raised the BDGIM VTEC values of 4.2% (2021), 8.0% (2022), 8.9% (2023), and 11.9% (2024) of all grid points, the by far most being located at higher latitudes, especially on the southern hemisphere. Since the area represented by IONEX grid points decreases with increasing latitudes (cp. Figure 5), the percentages of the affected areas are smaller: 2.6% (2021), 4.7% (2022), 5.6% (2023), and 7.7% (2024).

All of our evaluations are based on this modified BDGIM model, which will be referred to as the mBDGIM model in the following text.

Biases of the mBDGIM model with respect to the IGS reference model increase with increasing ionization (left panels of Fig. 13). In almost all regions, the annual bias averages show an underestimation of VTEC, especially strong in areas of the equatorial ionization anomalies and the southern hemisphere. Temporal maxima of this underestimation are observed in early 2023 and in almost all of 2024 (bottom left panel of Fig. 13).

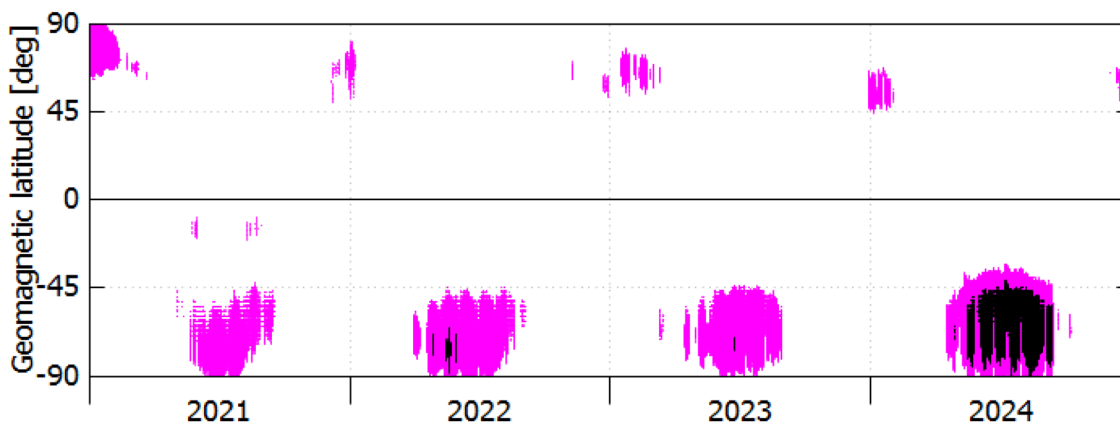


Fig. 12 Temporal and latitudinal distribution of BDGIM derived negative VTEC values in magenta and values even below -5 TECU in black

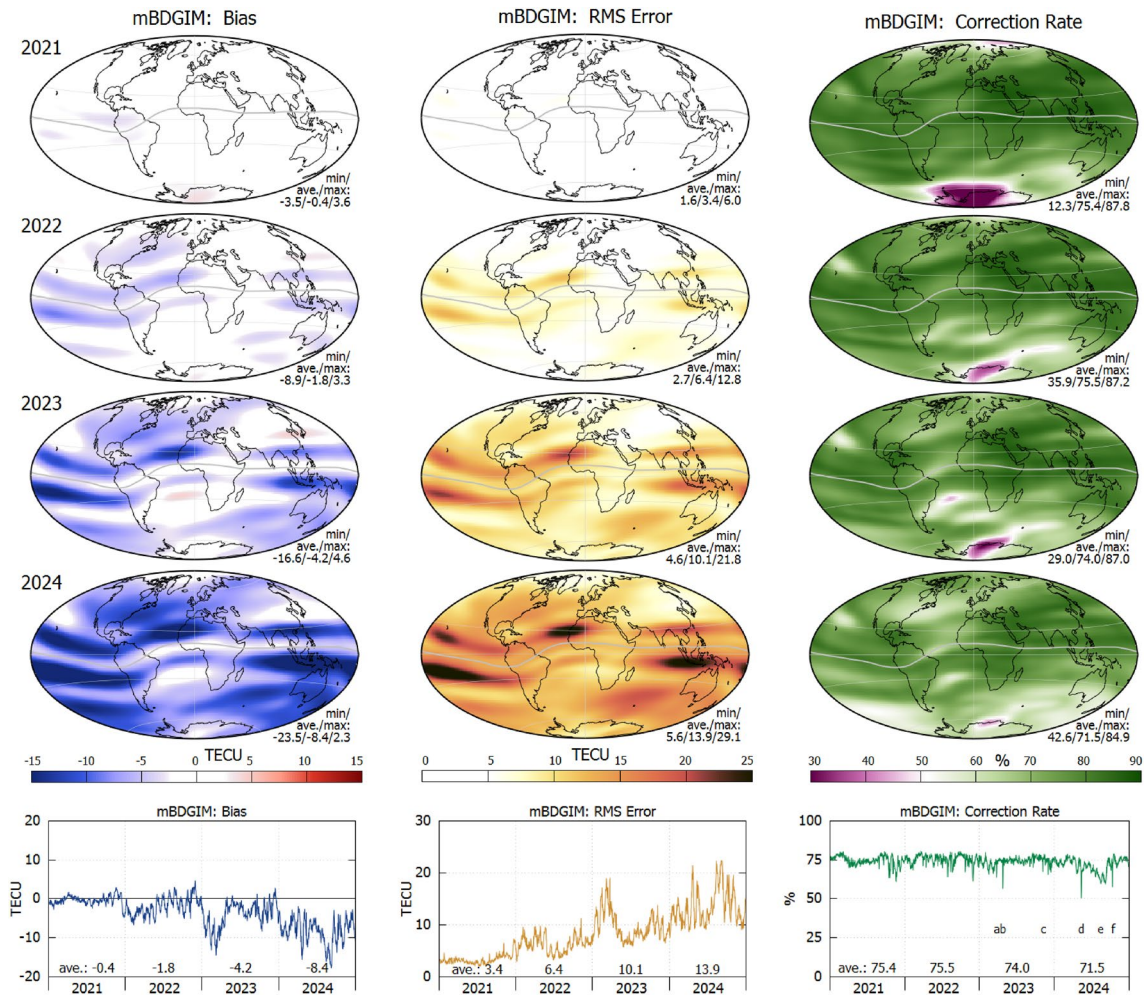


Fig. 13 Spatial distribution (annual averages, upper panels) and temporal distribution (daily global averages, bottom panels) of the statistical values bias (left), RMS error (center), and correction rate (right) for model mBDGIM

RMS errors increase from 2021 to 2024 (central panels of Fig. 13). They are larger in the equatorial region as compared to mid-latitude and polar regions. They are slightly larger in the southern hemisphere than in the northern hemisphere. In 2022 and 2023, larger global average RMS values are found in the first half of the year as compared to its second half (bottom central panel of Fig. 13).

Highest correction rates are found in the equatorial and mid-latitude regions (upper right panels of Fig. 13). In the polar region of the southern hemisphere, the annual mean correction rates are much worse, often below 50%.

Daily global average correction rates (bottom right panel of Fig. 13) are around 74%, but not as consistent as the NTCM-G percentages. In summer of 2024 they continuously decreased to a level of just 63% until, within a few days in the second week of November, they regained the earlier level of 75%. On a few single days, severe drops of the correction rates to less than 60% can be observed. Some of them can be attributed to the effects of geomagnetic storms, the largest

storms being labeled with letters a to f. The effects of these storms are discussed in more detail in a later section of this paper.

It is a striking feature of the mBDGIM model that smallest biases, smallest RMS errors and highest correction rates are found over China. There, the correction rates of the mBDGIM model reach 83.8% (2021), 81.4% (2022), 80.3% (2023), and 79.8% (2024) and are considerably higher than in other world regions, including other mid-latitude regions. The large regional performance differences of mBDGIM may be explained by the distribution of the GNSS observation stations of the BDS control segment which mainly relies on a regional tracking network in China and includes just a small set of global observation sites (Wang et al. 2021).

Combined NTCM-G/mBDGIM model

With two independent ionosphere prediction models of similar quality, namely NTCM-G and mBDGIM, the question arises as to whether a combined model might not produce even better results. A combination could consist of weighted averaging the VTEC values of both models according to the spatiotemporal distribution of the strengths and weaknesses of the individual models. We tried such combinations, but the result was no higher quality than averaging the VTEC values with equal weights. The averaging with equal weights according to

$$VTEC^{Comb}(t, \varphi, \lambda) = \frac{1}{2}(VTEC^{NTCM-G}(t, \varphi, \lambda) + VTEC^{mBDGIM}(t, \varphi, \lambda)) \tag{9}$$

produced the results shown in Fig. 14.

Spatial or temporal averages of the VTEC biases (left panels of Fig. 14) are identical to the arithmetic averages of the corresponding statistical figures of the individual models. Both models had shown an underestimation of the

ionization level, NTCM-G to a smaller extend, mBDGIM to a larger extend. Thus, the combined model shows negative bias values in the middle between the biases determined for the individual models. In almost all regions, the VTEC is underestimated, especially strong in areas of the equatorial ionization anomalies and in the southern hemisphere. Temporal maxima of this underestimation are observed in 2024 (bottom left panel of Fig. 14).

The annual mean RMS errors of the combined model are smaller than those of the individual models, except for 2024, where the RMS error of the combined model is slightly larger than that of NTCM-G. The annual means of the daily correction rates of the combined model are always larger than those of the individual models. Highest correction rates are found in the equatorial and mid-latitude regions (upper right panels of Fig. 14). In the polar region of the southern hemisphere the annual mean correction rate is worse, at some grid points even below 50%, but no negative correction rate values occur.

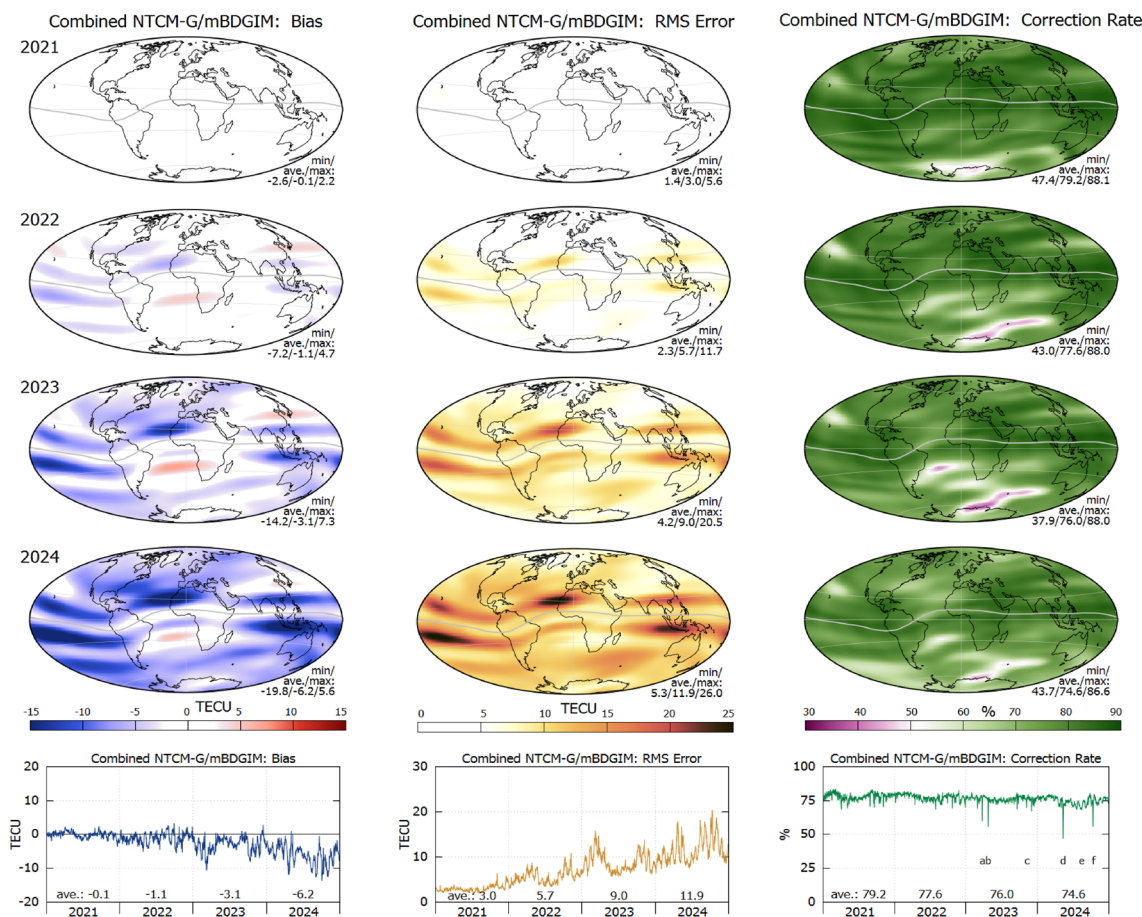


Fig. 14 Spatial distribution (annual averages, upper panels) and temporal distribution (daily global averages, bottom panels) of the statistical values bias (left), RMS error (center), and correction rate (right) for the combined model NTCM-G/mBDGIM

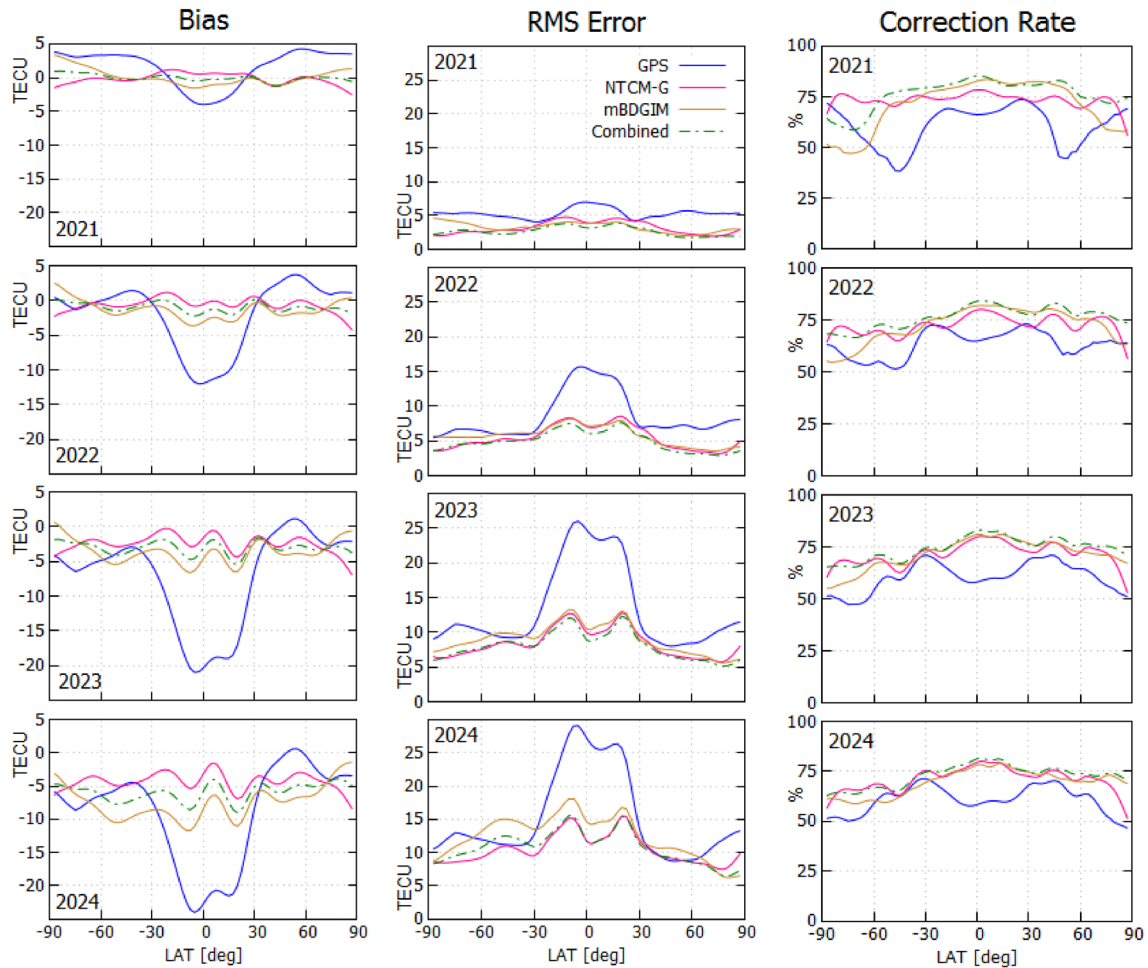


Fig. 15 Latitudinal dependencies of bias, RMS error and correction rate from 2021 to 2024

Table 2 Averaged statistical values for the 4-year period 2021–2024

Model	Bias [TECU]	RMS error [TECU]	Correction rate [%]
GPS	−5.8	13.8	58.5
NTCM-G	−1.6	8.3	73.5
mBDGIM	−3.7	9.3	74.1
Combined NTCM-G/ mBDGIM	−2.6	8.1	76.9

In conclusion, the combination of the two independent models NTCM-G and mBDGIM produces a model with slightly higher correction rates than the two original models.

Overall comparison

In order to enable the direct comparison of the 4 evaluated models Fig. 15 shows the latitudinal dependence of the three

statistical values: bias, RMS error, and correction rate. Only the GPS model exhibits significant biases in the equatorial region, which increase with solar activity. These biases also affect the RMS errors in this region. The NTCM-G and the BDGIM demonstrate similar performance levels. Their correction rates are typically greater than 70% in equatorial and mid-latitude regions. However, they decrease to nearly 50% for BDGIM in the southern polar region in 2021 and 2022 and for NTCM-G in the northern polar region in 2023 and 2024. In most latitude regions, the correction rates of the combined model surpass those of either the NTCM-G or the BDGIM. All models perform slightly better in the northern hemisphere than in the southern hemisphere.

Table 2 reports the average statistical values for the entire four-year period. The overall conclusion is that the GPS model performs worst. But still, it has a global VTEC correction rate of almost 60%. NTCM-G is somewhat superior to mBDGIM with respect to bias and RMS error. With 74.1%, the mBDGIM correction rate is slightly higher than that of NTCM-G. The combined model computed from

Fig. 16 Geomagnetic storm events in 2023 (a,b,c)

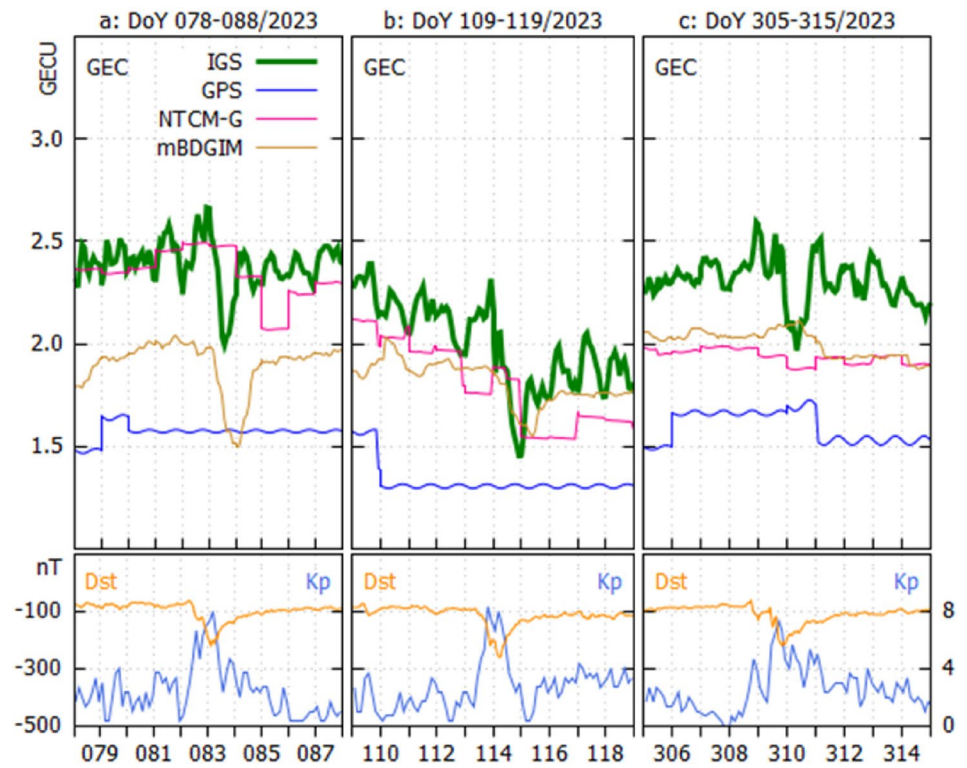
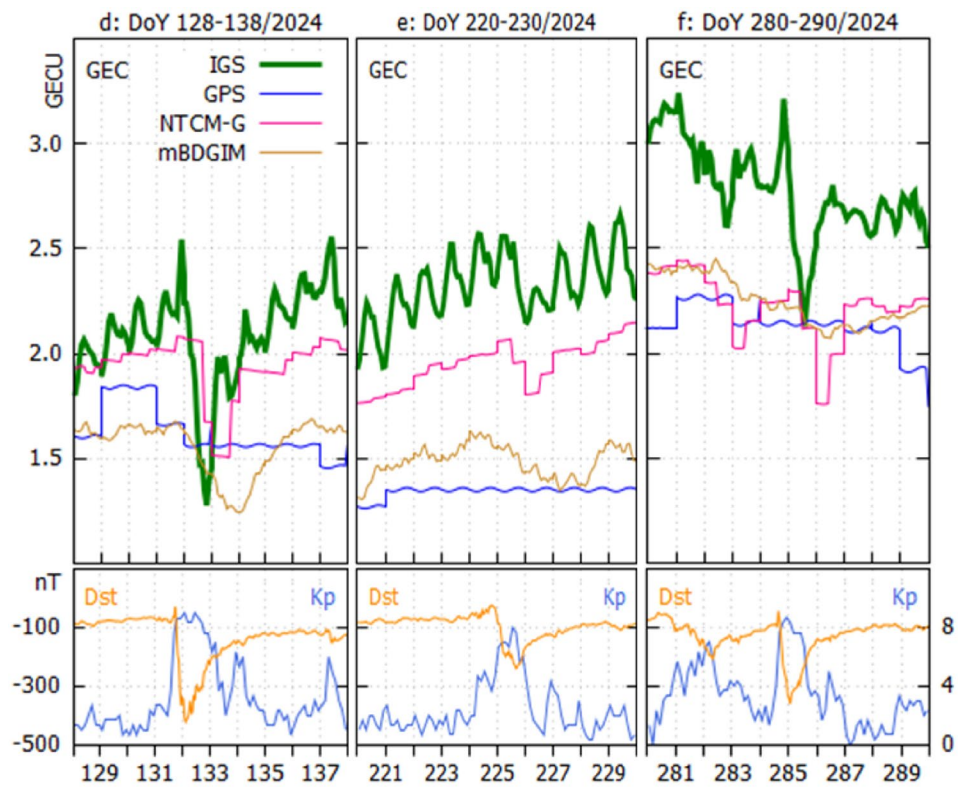


Fig. 17 Geomagnetic storm events in 2024 (d,e,f)



NTCM-G and mBDGIM VTEC values performs best with respect to RMS error and correction rate.

Geomagnetic storm events

The ionosphere reacts to solar and geomagnetic disturbances in several ways. High-latitude scintillation occurrence is highly correlated with geomagnetic storm events. But also, large-scale TEC variation in the form of enhancements and depletions are observed. Their spatial and temporal distribution is quite complex, with dependencies on season, hemisphere, latitudinal region, time of day and also longitude (Blagoveshchensky et al. 2018; Debchoudhury et al. 2021; Gulyaeva 2024; Mohamed et al. 2023). Such events pose a particular challenge to ionosphere prediction models that can hardly be solved.

We will look at the global effects of geomagnetic storms on TEC in the form of variation in GEC. The lower panels of Fig. 16 and 17 depict the histories of six such storms by the development of geomagnetic indices Dst and Kp. GEC derived from IGS ionosphere maps are shown in the upper panels, together with the GEC values of the three ionosphere prediction models GPS, NTCM-G, and mBDGIM. In order to increase the readability of the figures, GEC of the combined NTCM-G/mBDGIM model is not displayed, since this combination of the two models as performed by Eq. 9 results in GEC values that are always the arithmetic mean of the GEC values of the two original models.

The GEC time series of the IGS model reveal that with the onset of the storm an enhancement of GEC can be observed in most cases (a,b,d,f). In the main phase of the storm, GEC drops significantly by 20 to 30% (a,b,c,f), in case of the extremely strong storm in April 2024 (d) even by 50%. It takes 24 to 36 h for GEC to return to its original level.

Almost all GEC time series of the prediction models shown in Fig. 16 and 17 demonstrate the underestimation of global ionization by these models in 2023 and 2024. The responses of the ionosphere prediction models to the storm events differ. The GPS model does not react at all. NTCM-G reacts to the reduced ionization in all six cases. The time delays are often shorter than one day (b,c,e), in case of the two strongest storms in April and October 2024 (d,f) the delays reach 24 h, and in case of the storm in March 2023 (a) the reaction delay seems to be even longer. After a delay of 24 h and longer, however, the original GEC level has largely been restored so that the correction rate of NTCM-G remains low even for several hours after GEC recovery.

mBDGIM reacts to most storm events (esp. a,b,d) but completely misses out on two storms (c,f), among these the strong storm in October 2024. When a reaction is evident, the time delays range from 12 to 24 h and that although the model coefficients in the BDS navigation messages are

updated up to once per hour (cf. Table 1). As a consequence, the correction rates of mBDGIM are lower than usual during such storm events and also for several hours after the storm.

Geomagnetic storms pose the greatest challenge to ionosphere prediction models. Their performance could be improved by reducing their prediction times and increasing their update rates.

Conclusion and outlook

The evaluation of the three major GNSS ionosphere prediction models in the years 2021–2024 confirms that the Galileo coefficients applied with the NTCM-G algorithm and the BDS coefficients applied with a slightly modified BDGIM algorithm (mBDGIM) perform considerably better than the Klobuchar-GPS model. NTCM-G provides more consistent performance over time and space than mBDGIM. The latter produces a slightly higher correction rate than NTCM-G over the four-year period.

With two independent models of similar high quality, the question arose as to whether a combination of the two would produce even better results. And indeed, a simple combination by averaging the corresponding VTEC values slightly reduces the RMS errors and improves the correction rates.

Geomagnetic storms are a particular challenge for ionospheric prediction models. The three models evaluated responded differently to these events: GPS did not respond at all, Galileo/NTCM-G responded to all 6 major events in 2023 and 2024, and BDS/mBDGIM responded to some but not all of these events. Since all identified responses were time delayed by 12 to 24 h or even longer, they could not really improve the performance of the models. Correction rates of all models dropped significantly for those geomagnetic storms with strong effects on the ionization level of the ionosphere.

In conclusion, it can be recommended that single-frequency GNSS receivers with access to all GNSS should apply ionospheric corrections based on the ionosphere model coefficients and algorithms of Galileo/NTCM-G or BDS/mBDGIM, or a combination of both. The Klobuchar-GPS model should serve as a backup in case that Galileo and BDS navigation messages are not available.

The question remains as to which mapping function should be used to convert VTEC predictions to STEC. The mapping functions of NTCM-G and BDGIM differ by up to 4% for elevation angles above 30 deg and up to 7% for very low elevation angles. Further research should investigate whether such variations in the mapping functions have a significant impact on positioning performance.

Acknowledgements The International GNSS Service (IGS) is acknowledged for providing the IGS ionosphere model as one of its products.

Author contributions LW developed the study concept and prepared the first draft of the manuscript. LW and KT contributed to the data analysis and the discussion and interpretation of the results. Both authors critically reviewed and approved the final manuscript.

Funding Open Access funding enabled and organized by Project DEAL, an initiative of the Alliance of Science Organisations in Germany.

Data availability GNSS navigation messages and IGS ionosphere models are publicly available from NASA's Archive of Space Geodesy Data (CDDIS) (<https://cddis.nasa.gov>). Additional BDS navigation messages containing BDGIM model coefficients are publicly available from the Test and Assessment Research Center of the China Satellite Navigation Office (CSNO-TARC) (<https://www.csno-tarc.cn/>).

Declarations

Conflict of interest The authors declare no competing interests.

Open Access This article is licensed under a Creative Commons Attribution 4.0 International License, which permits use, sharing, adaptation, distribution and reproduction in any medium or format, as long as you give appropriate credit to the original author(s) and the source, provide a link to the Creative Commons licence, and indicate if changes were made. The images or other third party material in this article are included in the article's Creative Commons licence, unless indicated otherwise in a credit line to the material. If material is not included in the article's Creative Commons licence and your intended use is not permitted by statutory regulation or exceeds the permitted use, you will need to obtain permission directly from the copyright holder. To view a copy of this licence, visit <http://creativecommons.org/licenses/by/4.0/>.

References

- Afraimovich EL, Astafyeva EI, Oinats AV, Yasukevich YuV, Zhivetiev IV (2008) Global electron content: a new conception to track solar activity. *Ann Geophys* 26(2):335–344. <https://doi.org/10.5194/angeo-26-335-2008>
- Azpilicueta F, Brunini C (2009) Analysis of the bias between TOPEX and GPS vTEC determinations. *J Geod* 83(2):121–127. <https://doi.org/10.1007/s00190-008-0244-7>
- Azpilicueta F, Nava B (2021) On the TEC bias of altimeter satellites. *J Geod* 95(10):114. <https://doi.org/10.1007/s00190-021-01564-y>
- Blagoveshchensky DV, Maltseva OA, Sergeeva MA (2018) Impact of magnetic storms on the global TEC distribution. *Ann Geophys* 36(4):1057–1071. <https://doi.org/10.5194/angeo-36-1057-2018>
- Cahuasquí JA, Hoque MM, Jakowski N (2022) Positioning performance of the Neustrelitz total electron content model driven by Galileo Az coefficients. *GPS Solut* 26(3):93. <https://doi.org/10.1007/s10291-022-01278-4>
- CSNO (2019) BeiDou Navigation Satellite System Signal In Space Interface Control Document Open Service Signal B1I v3.0 (BDS-SIS-ICD-B1I-3.0), China Satellite Navigation Office
- Debhochdury S, Sardana D, Earle GD (2021) The Relative Importance of Geomagnetic Storm Signatures on the Total Electron Content Perturbations Over the Continental US. *JGR Space Physics* 126(5):e2020JA028125. <https://doi.org/10.1029/2020JA028125>
- Dettmering D, Heinkelmann R, Schmidt M (2011) Systematic differences between VTEC obtained by different space-geodetic techniques during CONT08. *J Geod* 85(7):443–451. <https://doi.org/10.1007/s00190-011-0473-z>
- EC (2016) Ionospheric Correction Algorithm for Galileo Single Frequency Users, Issue 1.2, European Commission
- EUSpace (2023) Galileo Open Service - Signal-in-Space Interface Control Document (OS SIS ICD), Issue 2.1
- Gioia C, Angrisano A, Gaglione S (2023) Neustrelitz total electron content model for Galileo performance: a position domain analysis. *Sensors* 23(7):3766. <https://doi.org/10.3390/s23073766>
- GSC (2022) NTCM-G Ionospheric Model Description Issue 1, European GNSS Service Center
- Gulyaeva TL (2024) Interaction of global electron content with the Sun and solar wind during intense geomagnetic storms. *Planet Space Sci* 240:105830. <https://doi.org/10.1016/j.pss.2023.105830>
- Guo M, Fan Y, Fan X, Sun G, Zhen J, Zhai W (2020) Performance Analysis of BDGIM. In: Sun J, Yang C, Xie J (eds) China satellite navigation conference (CSNC) 2020 Proceedings: Volume III. Springer Singapore, Singapore, pp 101–113. https://doi.org/10.1007/978-981-15-3715-8_10
- Hernández-Pajares M, Juan JM, Sanz J, Orus R, Garcia-Rigo A, Feltens J, Komjathy A, Schaer SC, Krankowski A (2009) The IGS VTEC maps: a reliable source of ionospheric information since 1998. *J Geod* 83(3–4):263–275. <https://doi.org/10.1007/s00190-008-0266-1>
- Hernández-Pajares M, Roma-Dollase D, Krankowski A, García-Rigo A, Orús-Pérez R (2017) Methodology and consistency of slant and vertical assessments for ionospheric electron content models. *J Geod* 91(12):1405–1414. <https://doi.org/10.1007/s00190-017-1032-z>
- Hoque MM, Jakowski N, Orús-Pérez R (2019) Fast ionospheric correction using Galileo Az coefficients and the NTCM model. *GPS Solut* 23(2):41. <https://doi.org/10.1007/s10291-019-0833-3>
- IS-GPS (2022) NAVSTAR GPS Space Segment/Navigation User Segment Interfaces (IS-GPS-200N)
- ISRO (2017) Indian Regional Navigation Satellite System, Signal in Space ICD for Standard Positioning Service, Version 1.1 (ISRO-IRNSS-ICD-SPS-1.1)
- Johnston G, Riddell A, Hausler G (2017) The International GNSS Service. In: Teunissen PJG, Montenbruck O (eds) Springer handbook of global navigation satellite systems. Springer International Publishing, Cham, pp 967–982. https://doi.org/10.1007/978-3-319-42928-1_33
- JSC (2016) GLONASS Interface Control Document, General Description of Code Division Multiple Access Signal System, Edition 1.0, Russian Space System (JSC)
- Klobuchar J (1987) Ionospheric Time-Delay Algorithm for Single-Frequency GPS Users. *IEEE Trans Aerosp Electron Syst* AES 23(3):325–331. <https://doi.org/10.1109/TAES.1987.310829>
- Krankowski A, Hernández-Pajares M (2021) Ionosphere Working Group Technical Report 2020. In: IGS Technical Report 2020. Astronomical Institute, University of Bern, pp 203–208. <https://doi.org/10.48350/169536>
- Li M, Yuan Y, Wang N, Li Z, Huo X (2018) Performance of various predicted GNSS global ionospheric maps relative to GPS and JASON TEC data. *GPS Solut* 22(2):55. <https://doi.org/10.1007/s10291-018-0721-2>
- Liu A, Wang N, Dettmering D, Li Z, Schmidt M, Wang L, Yuan H (2023) Using DORIS data for validating real-time GNSS ionosphere maps. *Adv Space Res* 72(1):115–128. <https://doi.org/10.1016/j.asr.2023.01.050>
- Matzka J, Stolle C, Yamazaki Y, Bronkalla O, Morschhauser A (2021) The Geomagnetic K_p Index and Derived Indices of Geomagnetic Activity. *Space Weather* 19(5):e2020SW002641. <https://doi.org/10.1029/2020SW002641>

- Mayaud PN (1980) Derivation, Meaning, and Use of Geomagnetic Indices. American Geophysical Union, Washington, D.C. <https://doi.org/10.1029/GM022>
- Mohamed HS, Amory-Mazaudier C, Panda SK, Shalabiea OM, Mahrous A (2023) Delayed response of low latitudes TEC during thirty-six geomagnetic storms from 2014 to 2017. *J Atmos Solar Terr Phys* 250:106109. <https://doi.org/10.1016/j.jastp.2023.106109>
- Morton YJ, Yang Z, Breitsch B, Bourne H, Rino C (2020) Ionospheric Effects, Monitoring, and Mitigation Techniques. In: Morton YJT, Diggelen F, Spilker JJ, Parkinson BW, Lo S, Gao G (eds) Position, navigation, and timing technologies in the 21st century, Wiley, pp 879–937. <https://doi.org/10.1002/9781119458449.ch31>
- Orús R, Hernández-Pajares M, Juan JM, Sanz J (2005) Improvement of global ionospheric VTEC maps by using kriging interpolation technique. *J Atmos Solar Terr Phys* 67(16):1598–1609. <https://doi.org/10.1016/j.jastp.2005.07.017>
- QZSS (2021) Quasi-Zenith Satellite System Interface Specifications: Satellite Positioning, Navigation and Timing Service (IS-QZSS-PNT-004)
- Schaer S (1999) Mapping and Predicting the Earth's Ionosphere Using the Global Positioning System. Schweizerische Geodätische Kommission, Zürich, Switzerland
- Schaer S, Gurtner W, Feltens J (1998) IONEX: The IONosphere Map EXchange Format, Version 1
- Setti PT, Da Silva CM, Alves DBM (2025) Assessing GNSS ionospheric models at low latitudes: BDGIM, NeQuick-G, and Klobuchar. *GPS Solut* 29(1):15. <https://doi.org/10.1007/s10291-024-01761-0>
- Wang N, Li Z, Yuan Y, Huo X (2021) BeiDou Global Ionospheric delay correction model (BDGIM): performance analysis during different levels of solar conditions. *GPS Solut* 25(3):97. <https://doi.org/10.1007/s10291-021-01125-y>
- Yasyukevich YV, Zatolokin D, Padokhin A, Wang N, Nava B, Li Z, Yuan Y, Yasyukevich A, Chen C, Vesnin A (2023) Klobuchar, NeQuickG, BDGIM, GLONASS, IRI-2016, IRI-2012, IRI-Plas, NeQuick2, and GEMTEC ionospheric models: a comparison in total electron content and positioning domains. *Sensors* 23(10):4773. <https://doi.org/10.3390/s23104773>
- Yuan Y, Wang N, Li Z, Huo X (2019) The BeiDou global broadcast ionospheric delay correction model (BDGIM) and its preliminary performance evaluation results. *Navigation* 66(1):55–69. <https://doi.org/10.1002/navi.292>
- Zhao K, Yan W, Yang X, Yang H, Wei P (2020) BDGIM performance evaluation based on iGMAS global tracking network. *Adv Space Res* 66(9):2168–2178. <https://doi.org/10.1016/j.asr.2020.07.037>
- Zhang Q, Liu X, Liu Z, Hu Z, Zhao Q (2022) Performance evaluation of BDS-3 ionospheric delay correction models (BDSK and BDGIM): First year for full operational capability of global service. *Adv Space Res* 70(3):687–698. <https://doi.org/10.1016/j.asr.2022.05.009>
- Zhang Q, Zhao Q (2023) Negative VTEC with spherical harmonic expansion model under different solar activity conditions. *Adv Space Res* 71(3):1806–1817. <https://doi.org/10.1016/j.asr.2022.09.030>
- Zhu Y, Tan S, Zhang Q, Ren X, Jia X (2019) Accuracy evaluation of the latest BDGIM for BDS-3 satellites. *Adv Space Res* 64(6):1217–1224. <https://doi.org/10.1016/j.asr.2019.06.021>

Publisher's Note Springer Nature remains neutral with regard to jurisdictional claims in published maps and institutional affiliations.